ENEL 697

Winter 2007

Detection and Segmentation of Pelvic Girdle in CT Images of Children with Neuroblastoma

Shantanu Banik

1 Abstract

Neuroblastoma is the most common extra-cranial, solid, malignant tumor in children. Advances in radiology have made possible the detection and staging of the disease. Segmentation and analysis of the tissue composition of the tumor can assist in quantitative assessment of the response to chemotherapy and in the planning of delayed surgery for resection of the tumor. But, due to the heterogeneous tissue composition of neuroblastoma, ranging from low-attenuation necrosis to high-attenuation calcifications, segmentation of tumor mass is a challenging problem. So, in attempt to segment the tumor mass directly results in severe leakage in contiguous anatomical structure such as the heart, the liver, the kidneys and many other organs and tissues possess CT characteristics that are similar to those of the tumoral tissues. It has been observed that some preprocessing steps reduced the potential for leakage through the heart and provides an effective landmark for the identification of additional abdominal organs. Identification of diaphragm and the pelvic girdle result in segmentation of the abdominal cavity and removed the probability of leakage outside that region and is expected to reduce the false positive rates in the tumor segmentation.

After removing air, fat and muscle and other peripheral artifacts and thresholding that image I obtained a rough estimate of the pelvic girdle. By incorporating reconstruction in the fuzzy region growing and applying differnt morphological image processing technique I was able to get a refined model of pelvic girdle. As pelvic girdle is made up of bones, those are supposed to have high Hounsfield unit values and high gray level values in the images. But due to the fact that neuroblastoma is a child disease and the pelvic girdle bones may not be fully developed (both in structural and tissue composition characteristics), in many cases, it caused intermixing the values with other contiguous and neighboring organs and tissues of close or same gray levels. In addition, most of the times, the pelvis bones appearred as disjoint regions which made the task more complicated. In my project, based on fuzzy mapping and reconstruction I have studied several detection and segmentation methods of pelvic girdle using automatically selected seeds in the CT images.

2 Neuroblastoma

Neuroblastoma is a malignant tumor of neural crest origin that may arise anywhere along the sympathetic ganglia or within the adrenal medulla [1, 2]. Neuroblastoma belongs to an enigmatic group of neoplasms, which have the highest rate of spontaneous regression of all human malignant neoplasms, yet one of the poorest outcomes when presenting as disseminated disease in children.

Neuroblastoma is the most common extra-cranial solid malignant tumor in children; it is the third most common malignancy of childhood, surpassed in incidence only by acute leukemia and primary brain tumors [3]. It accounts for 8-10% of all childhood cancers, but is responsible for 15% of all cancer-related deaths in the pediatric age group [1, 4, 5]. The median age of incidence is two years, and 90% of the diagnosed cases are in children under the age of five years [2]. Seven to 10 new cases per million children younger than 15 years of age are annually diagnosed in Canada and the United States [6, 7, 8].

Sixty-five percent of neuroblastomas are located in the abdomen; approximately two-thirds of these arise in the adrenal gland. Fifteen percent are thoracic, usually located in the sympathetic ganglia of the posterior mediastinum. Between 10 and 12% of neuroblastomas are disseminated without a known site of origin [3].

The overall survival rate for all stages of neuroblastoma is 72% if the patient is under the age of one year of age, 28% for children between the ages of one and two, and 12% for those older than two years of age [3]. The improved prognosis of infants with early-stage neuroblastoma has prompted the initiation of infant-screening studies. Mass screenings of infants for neuroblastoma have been studied systematically in Japan, North America, and Europe [9]. The results of the trials have shown an increase in the detection of neuroblastoma cases; however, despite this increased incidence in the screen group, the neuroblastoma mortality rates were unchanged by the screening [9].

2.1 Clinical Staging

The main prognostic factors in neuroblastoma are the age of the patient and the stage of the disease at diagnosis. The detection of neuroblastoma at an early stage of the disease generally leads to a favorable prognosis. The site of primary involvement of neuroblastoma is also important in the overall prognosis. Tumors arising in the abdomen and pelvis have the worst prognosis, with adrenal tumors having the highest mortality. Thoracic neuroblastoma has a better overall survival rate of 61%, compared to a survival rate of 20% with abdominal tumors [3].

As with other cancers, a formal system for clinical staging of neuroblastoma is useful for prognostication and for comparing results of treatment. The International Neuroblastoma Staging System (INSS) [10] takes into account radiologic findings, surgical resectability, lymph node involvement, and bone marrow involvement. Based on these criteria, the extent of the neuroblastoma disease is classified into four main stages. Localized tumors are divided into stages 1,2, and 3, while widespread disease in infants is divided into 2 categories, stage 4 and 4S [11].

2.2 Imaging

CT and MRI are currently the imaging modalities of choise for characterization of neuroblastoma. CT is essential for the confirmation, localization, and staging of neuroblastoma, whether the tumor is abdominal, pelvic, thoracic, cervical, or intracranial in location. The sensitivity for detection of abdominal neuroblastoma on CT is virtually 100% [7, 3]. Tumor size, location, composition, and relationship to adjacent structures are all adequately demonstrated on CT [7]. CT may demonstrate prevertebral tumor extension across the midline, encasement of major vessels, invasion or displacement of the pancreas, and retrocrural extension into the chest.

On computed tomography (CT) exams, abdominal neuroblastoma is seen as a mass of soft tissue, commonly suprarenal or paravertebral, usually irregularly shaped, lobulated, and lacking a capsule [3]. Calcifications are readily detectable on CT and are present in about 85% of cases of neuroblastoma. Calcifications are usually dense, amorphous, and mottled in appearance.

MRI is well suited for the evaluation of children with neuroblastoma and probably offers sensitivity equal to that of CT. Demonstration of vascular anatomy with MRI is usually superior to that with CT. The tissue characterization that MRI provides presents useful information for differentiating neoplastic disease from normal structures. Major drawbacks of the modality include expense, long imaging time, and the usual requirement for sedation [7]. As such, CT is still the primary imaging modality.

In CT, the physical characteristics of tissue are displayed using a normalized unit known as a CT number. The CT number is dependent on the linear attenuation coefficient, ρ, of a tissue and is calculated relative to water. The tissue density is represented by a CT number, defined in Equation 1 as:

$$\text{CT number} = k(\rho - \rho_w)/\rho. \tag{1}$$

A CT number is a normalized measure of the tissue density, represented as the linear attenuation coefficient ρ, relative to the linear attenuation coefficient of water, ρ_w. The parameter k is a scaling constant, which is set to 1000 to obtain a CT number in terms of Hounsfield units (HUs). Several tissue types and their corresponding Hounsfield value are presented in Table 1.

Table 1: Mean and standard deviation of common abdominal tissues in Hounsfield Units (HU).

	CT value, HU	
Tissue	mean	SD
Air	-1006	2
Fat	-90	18
Bile	+16	8
Kidney	+32	10
Pancreas	+40	14
Blood (aorta)	+42	18
Muscle	+44	14
Spleen	+46	12
Necrosis	+45	15
Liver	+60	14
Viable tumor	+91	25
Marrow	+142	48
Calcification	+345	155
Bone	+1005	103

This table has been reproduced from [12].

2.3 Computer-aided Analysis

In the treatment of patients with neuroblastoma, the ultimate goal or the treatment of choice is the complete surgical resection of the tumor mass [3]. However, due to the size or extension of the mass, radiation therapy or chemotherapy may first be required to shrink the tumor before resection can be performed. As such, the evaluation of the tumor mass is an important measure of the response of the disease to therapy. In this context, computer-aided analysis in the form of tumor segmentation can be beneficial to the radiologist, providing a quantitative, reproducible evaluation of the tumor mass. Advances in radiology have made possible the detection and staging of the disease. Segmentation and analysis of the tissue composition of the tumor can assist in quantitative assessment of the response to chemotherapy and in the planning of delayed surgery for resection of the tumor.

3 Background

Due to the heterogeneous tissue composition of neuroblastoma, ranging from low-attenuation necrosis to high-attenuation calcifications, segmentation of tumor mass is a challenging problem. The tumor is usually composed of inhomogeneous tissue types, some of which possess strong similarities in computed tomographic characteristics to contiguous nontumoral tissues. So, in attempt to segment the tumor mass directly results in severe leakage in contiguous anatomical structure such as the heart, the liver, the kidneys and many other organs and tissues possess CT characteristics that are similar to those of the tumoral tissues. Furthermore, viable tumor, necrosis, fibrosis, and normal tissues are often intermixed. Rather than attempt to separate these tissue types into distinct regions, Rangayyan et al.[13] proposed to explore methods to delineate the normal structures expected in abdominal CT images, remove them from further consideration, and examine the remaining parts of the images for the tumor mass. In order to improve the segmentation result Deglint et al.[14] identified several potential sources of leakage in the body and developed method to remove them from further consideration. Previous work on the segmentation of the primary tumor mass by Vu et al.[15] focused on the removal of various problematic tissues and structures prior to segmentation using different segmentation algorithms. In that work, Vu et al.[15] proposed and implemented an improved segmentation procedure of the peripheral muscle, identification and extraction of the diaphragm and the subsequent removal of the thoracic cavity. That preprocessing method removed the potential for leakage through the heart and provides an effective landmark for the identification of additional abdominal organs. Incorporating opening by reconstruction by using region marker that work showed an excellent result in terms of average true positive rate (82.2%) but had a poor result in terms of average false positive rate (1281.6%)[15] due to leakage in other abdominal tissues and organs.

So, in addition, the identification and segmentation of pelvic girdle will result in the abdominal cavity between the diaphragm and the pelvis and is expected to reduce the probability of leakage and the high false positive rates in the region growing method.

4 Image Segmentation

Digital images may be manipulated in a variety of ways for many applications.The different manipulations can be categorized as *image processing* and *image analysis*. Segmentation, a form of image processing, is the process of partitioning an image into regions representing the different objects in the image. Segmentation of objects, especially in medical images is a difficult task. Generally, boundaries of the desired objects on surrounding features in an image are subtle, or region corresponding to the objects of interest lack a sufficient level of similarity to achieve accurate segmentation. Besides the same object may be represented by a group of disjoint regions with varying characteristics. Futhermore, noise and artifacts degrade the image and interfere with object definition.

A number of segmentation techniques are used in this project to obtain the pelvis and are presented here in brief.

4.1 Thresholding

Gray level thresholding segments an image based on the image's value at each point (x, y) relative to a threshold value, T. It is the simplest method of image segmentation relying only

on the point values of the pixels. A threshold can be global or local. In the simplest case of thresholding, also known as *binarization*, a single threshold is specified for an image $f(x, y)$ and the result is defined as [16]

$$g(x,y) = \begin{cases} 1 & \text{if } f(x,y) > T \\ 0 & \text{if } f(x,y) \leq T \end{cases}$$

(2)

where $T \epsilon G$.

Thresholding requires knowledge of the expected gray levels of the objects of interest and the background, in order to be effective. In many cases, several objects of interest may possess different gray-scale values, requiring the use of multiple thresholds to achieve their individual segmentation. The approach is known as *multi thresholding*. Still, selection of appropriate threshold is a difficult task and that selection need to be made adaptive sometimes for better result. In the case of CT images, several organs within the body have similar characteristics (see table 1), and thresholding may fail to yield the individual structures.

4.2 Region Growing

Region based segmentation makes use of spatial information: methods in this category rely on the posthulate that neighboring pixels within a region have similar characteristics. The ultimate goal of segmentation is to group pixels (or voxels) into regions, such that the resulted objects are homogeneous, consisting of pixels corresponding to the same true object. Such methods may be based on either a measure of similarity or discontinuity between a pixel and its neighborhood.

Region-growing is a segmentation procedure in which the desired objected is delineated by the successive aggregation of voxels that satisfy a given inclusion or homogeneity criterion and that are connected to the current estimate spatially. This homogeneity criterion should be selected such that it is broad enough to include the desired regions, but strict enough to ignore dissimilar regions. The assumption used to govern such a procedure is that the desired region is homogeneous, consisting of similar values. Therefore, because of the homogeneity of the region, a region-growing procedure is quite suitable. By convention, there are two primary types of neighborhoods for a 2-D image: 4-connected and 8 connected and for a 3-D image: 6-connected and 26-connected are widely used.

The major limitations of region growing are the difficulty in specifying seed pixels that properly represent the characteristics of the regions of interest, in defining suitable inclusion criteria for aggregating pixels and formulation of a stopping rule. In the case of segmentation of pelvic girdle, region growing may leak to neighboring structures that possess similar CT characteristics.

4.3 Fuzzy Segmentation

Traditional methods of segmentation, such as thresholding and region growing, aim to partion an image in a "crisp" manner. That is, the image is divided into regions that are either absolutely part of the region of inerest or not. Such an approach of "all or nothing" is effective only when the objects are clearly defined. In images, where the object boundaries

are ill-defined as in medical images, the structure of such methods need to be made more flexible. Fuzzy sets are a logical choice for such imprecision because they serve as a natural framework for the purpose of segmentation.

A fuzzy set $\mathcal{A}$ is represented by a membership function $m_{\mathcal{A}}$ which maps numbers into the entire unit interval $[0, 1]$.The value $m_{\mathcal{A}}(r)$ is called the *grade of membership* of r in $\mathcal{A}$. This function has three properties of *normality*, *monotonicity* and *symmetry*. The unnormalized gaussian function, defined as

$$m_{\mathcal{A}}(r) = exp\{-(r-\mu)^2/2\sigma^2\}$$

(3)

is such an membership function satisfying the properties above.

In the context of image segmentation, fuzzy sets provide a very powerful tool. It could be used to quantify the similarity of image elements to the objects of interest. Using the mapping function in equation 3, the desired structures will appear as bright regions of high membership values, whereas the undesired structures will be faint, possessing a low degree of similarity or membership. The membership function operates globally; it identifies all elements of the image that demonstrate the characteristics of the object of interest. As a result several potential candidates may arise for the desired objects.

4.3.1 Fuzzy Connectivity

A method that employs the concept of fuzzy connectedness has been introduced in [17]. This method examines not only the homogeneity of neighboring pixels, but also the notion of "hanging togetherness" of image elements, to capture voxels that are located in different spatial regions. The aim is to capture the properties of graded composition and hanging togetherness within the notion of a "fuzzy object" [17].

The connectedness between two points c and d is a function of all possible paths connecting the two points. Each path is formed by a sequence of links between successive adjacent points in the path. The strength of each link is simply the affinity between the two adjacent points in the link and the strength of each path is the weakest link along the path. The strength of the connection between point c and d is called connectivity, and is given by the strongest path over all possible paths between the points, c and d.

Bloch [18] described the degree of connectedness between two arbitrary points c and d of a fuzzy set characterized by the fuzzy membership μ to be:

$$\eta_{\mu}(c,d) = \max_{p \epsilon P_{cd}} [\min_{1 \leq i \leq n} \mu(c_i)] \tag{4}$$

For two arbitrary points c and d, c_i, $1 \leq i \leq n$ represents the successive adjacent elements in a path joining the two points. Therefore, $c = c_1$ and $d = c_n$.

In the project, I have applied morphological reconstruction method in lieu of fuzzy connectivity to the image mapped using the fuzzy membership function.

4.4 Morphological Technique

Mathmatical morphology [19, 20] refers to a branch of nonlinear image processing that focuses on the analysis of geometrical structures within an image. It is based on conventional set theory, which serves as a framework for image processing and analysis. In addition to image segmentation, morphology provides methods for image enhancement, restoration, edge detection , texture analysis and shape analysis. It is based on analyzing the effects of applying a geometric form known as *structuring element* to the given image and the goal is to probe the image with that structuring element and quantify the manner in which the structuring element fits or does not fit within the image.

Two fundamental morphological operations are *erosion* and *dilation* [21] which are based on *Minkowski algebra* [19, 20]. Several additional secondary operations such as *opening* and *closing*, are made possible by combining the elementary operators sequentially.

4.4.1 Erosion

The translation invariant erosion operation is known as *Minkowski subtraction* in set theory [19, 21], and is defined as

$$F \ominus B = \{h \epsilon \mathbb{R}^n \mid (B + h) \subseteq F\} = \bigcap_{b \epsilon B} F - b \tag{5}$$

where F and B are subsets of $\mathbb{R}^n$, B is the structuring element for the purpose of eroding F, and h is an element of the set of all possible translations. For digitized image, F and B are subsets of $\mathbb{Z}^n$ and $h \, \epsilon \, \mathbb{R}^n$. In terms of set theory, $F \ominus B$ is formed by translating F by every element in B and taking the intersection of the results obtained.

Logically, the procedure works as follows: The value of the output pixel is the minimum value of all the pixels in the input pixel's neighborhood defined by the structuring element. In a binary image, if any of the pixels is set to 0 within the neighborhood, the output pixel is set to 0. So, the operation has the effect of "shrinking" the original object according to the structing element when the structuring element contains the origin.

4.4.2 Dilation

The translation invariant dilation operation is known as *Minkowski addition* in set theory [19, 21], and is defined as

$$F \oplus B = \{h \epsilon \mathbb{R}^n \mid (\breve{B} + h) \bigcap F \neq \phi\} = \bigcap_{b \epsilon B} F + b \tag{6}$$

where $\breve{B} = -b \mid b \epsilon B$ is the reflection of B with respect to the origin ϕ is the null set. In terms of set theory, a dilation is the union of all copies of F translated by every element in B. So, logically, the value of the output pixel is the maximum value of all the pixels in the input pixel's neighborhood defined by the structuring element. In a binary image, if any of the pixels is set to the value 1, the output pixel is set to 1. The dilation has the effect of "expanding" the original object when the structuring element contains the origin.

4.4.3 Morphological Opening and Morphological closing

Morphological opening and closing are achived by the sequential applications of erosion and dilation. Morphological opening is obtained by applying an erosion followed by a dilation as,

$$F \circ B = (F \ominus B) \oplus B \tag{7}$$

On the otherhand, morphological closing is achived by applying a dilation followed by an erosion as,

$$F \bullet B = (F \oplus B) \ominus B \tag{8}$$

Opening has the effect of removing objects or details smaller than the structuring element B, while smoothing the edges of the remaining objects. It also disconnects objects that are connected by branches that are smaller than the structuring element.

On the otherhand, closing has the effect of filling in holes and intrusions that are amaller than the structuring element.

4.4.4 Reconstruction

"Reconstruction" is an operation provided by mathematical morphology that is useful in evaluating the connectivity of objects in an image. This is an iterative procedure that can extract regions of interest from an image identified or selected by a set of "markers" in the image. Reconstruction operates on the notion of connection cost, or the minimum distance between specific poits in a defined set.

The reconstruction transformation simply extracts the connected components of an image which are "marked" by another image [22]. It can be seen as a series of geodesic dilations of a marker, J, constrained by a mask, I [22]. The elementary geodesic dilation of $\delta_I^{(1)}(J)$ of a binary image $J \leq I$ under I is defined as

$$\delta_I^{(1)}(J) = (J \oplus B) \wedge I. \tag{9}$$

In equation 9, $\wedge$ represents the pointwise minimum and $(J \oplus B)$ is the dilation of J using a flat structuring element B.

The definition of binary reconstruction can be extended to grayscale images. The grayscale geodesic dilation of size $n \geq 0$ is then given by

$$\delta_I^{(n)} = \underbrace{\delta_I^{(1)} \circ \delta_I^{(1)} \circ \cdots \circ \delta_I^{(1)}(J)}_{n!times}. \tag{10}$$

The grayscale reconstruction of I from J, denoted as $\rho_I(J)$, is obtained by dilating J, constrained by the mask I [22], which is formally defined as:

$$\rho_I(J) = \bigvee_{n \geq 1} \delta_I^{(n)}(J). \tag{11}$$

Using these image processing techniques I have tried to detect and segment the pelvic girdle in CT images.

5 Preprocessing Steps

Before getting into the original project work I have applied the preprocessing steps proposed by Vu et al. [15] and eliminated air, fat, skin and peripheral muscle from further consideration. In addition, I have used the the method proposed by Rangayyan and Deglint [13] to extract the spinal canal region which is used in the project to assist automatic seed selection.

5.1 Removal of Air

Air, by definition, has a CT number of -1000 HU. To remove air external to the body, the CT volume is thresholded with the range -1200 to 5 HU to account for variations due to noise and partial volume averaging. 2-D binary reconstruction using an 4-connected neighborhood is applied to each slice of CT volume where the four corner pixels of each slice are used as the markers and each thresholded slice is used as mask. After completion of reconstruction, the resulted volume is morphologically closed using a 'disk' type structuring element of radius 10 to remove material external to the body, such as patient table, blanket and tubes connected to intravnous drips.

5.2 Removal of Skin and Fat

The skin has a usual thickness of one to three millimeters. Using the parameter for expected skin thickness, the boundary of the body obtained via segmentation of air region was shrunk using 3D morphological operation to remove skin.

The fat has a CT value of $\mu = -90$ HU and $\sigma = 18$ [23, 24]. Peripheral fat around the abdomen varies in thickness from 3 mm to 8 mm in children. Following the removal of skin, voxels within a distance of 8 mm from the inner skin boundary are examined for inclusion as fat. If these voxels fall within the range of $-90 \pm 3 \times 18$HU, they are clasified as fat. In this procedure, partial volume averaging has been taken into account.

The regions of partial volume effect are calculated based on the lowest and highest value parameters, which determine the range of values that are particular to the partial volume effect. Within a 5x5 window, the max and min are calculated and if they are above threshold, then the center pixel is compared against the lowest and highest values to see if it is within the range that we're interested in.

5.3 Removal of Peripheral Muscle

Peripheral muscle has a mean CT value of $\mu = +44HU$ and $\sigma = 14HU$ [23, 24] and a varying thickness of 6 mm to 10 mm in abdominal sections. As in case of peripheral fat, voxels found within 10 mm of the inner fat boundary and within the range of $44 \pm 2 \times 14$ HU are classified as peripheral musle.

5.4 Detection of Spine

The method proposed by Rangayyan and Deglint [13] was employed to obtain the spinal canal. After removal of external and peripheral material, the CT volume was thresholded[15] at $+800 - 2 \times 103HU$to obtain binarized bone volume. The data volume was then cropped to remove CT slices containing the head, neck and pelvis for consideration and to consider the vertibral column in the thoracic and abdominal column only. The cropped and binarized

bone volume was subjected to a 3D derivative operation to extract the edge map representing the bone boundary. The Hough transform was then applied to the edge map with the radius parameter limited to the range 6 to 10 mm. To make certain the appropriate circle is identified, the center voxel of the best fitting circle was examined to ensure that it was located within the spinal canal. After determining the appropriate center, the reconstruction technique was applied in 3D to delineate the spinal canal. Subsequently, the fuzzy region was thresholded at T=0.80 and the region was morphologically closed in 3D using a tubular structuring element of size $2mm \times 2mm \times 5mm$.

Different morphological techniques, fuzzy mapping and reconstruction have been used extensively in the preprocessing steps described above. For the present project work, I have not used the seed selection procedure for spinal canal described earlier. Rather, I have used the selected seed points previously obtained by that method to grow the spinal canal region. The rest other preprocessing steps were implemented as indispensable part of the project following the described procedure by Vu et al.[15].

The result of the preprocessing steps are shown in figure 1. Only one slice is shown as a representative case.

6 Pelvic Girdle Detection and Segmentation

I have studied different detection and segmentation methods of pelvic girdle in the CT images by thresholding the resulted images after removing air, fat and muscle and other peripheral artifacts. Using that thresholded images I have tried to incorporate reconstruction in the preprocessed CT slices to segment the pelvic girdle. As pelvic girdle is made up of bones, those are supposed to have high Hounsfield unit values and high gray level values in the images. But due to the fact that neuroblastoma is a child disease and the pelvic girdle bones may not be fully developed (both in structural and tissue composition characteristics) in many cases, there is a high possibility of intermixing the values with other contiguous and neighboring organs and tissues of close or same gray levels. In my project, I have searched for appropriate and effetive algorithms to detect and segment the pelvic girdle in CT images with a view to improve the segmentation of Neuroblastoma tumor mass in terms of reducing false positive rates.

The CT exams used in this work are anonymous cases from the Alberta Children's Hospital. The 10 exams are of four patients of age two weeks to 11 years with varying number of slices. The exams were acquired using GE Medical System Lightspeed QX/i or a QX/i Plus heical CT scanner. Almost all the CT exams include contrast enhancement. The data have an interslice resolution of 5 mm and the intraslice resolution varies from 0.35 mm to 0.55 mm. The computer used to process the exams is a Dell Precision PWS490 with Intel(R) Xeon(TM) 3.00 GHz processor and 4 GB of RAM.

6.1 Seed Selection

The detected spinal canal region was used as a mean of seed selection. The last slice that contains the spinal canal region was taken as reference slice number and the seeds were selected from 2 slice back from that slice number. The reson for choosing that slice is that it was found to be a good position to select the seeds for pelvis for all the CT exams.

At first, the resulting image after removing air, skin, fat and muscle was thresholded at 300 HU value. In case of two seeds application, for a 512×512 CT image, the searching area

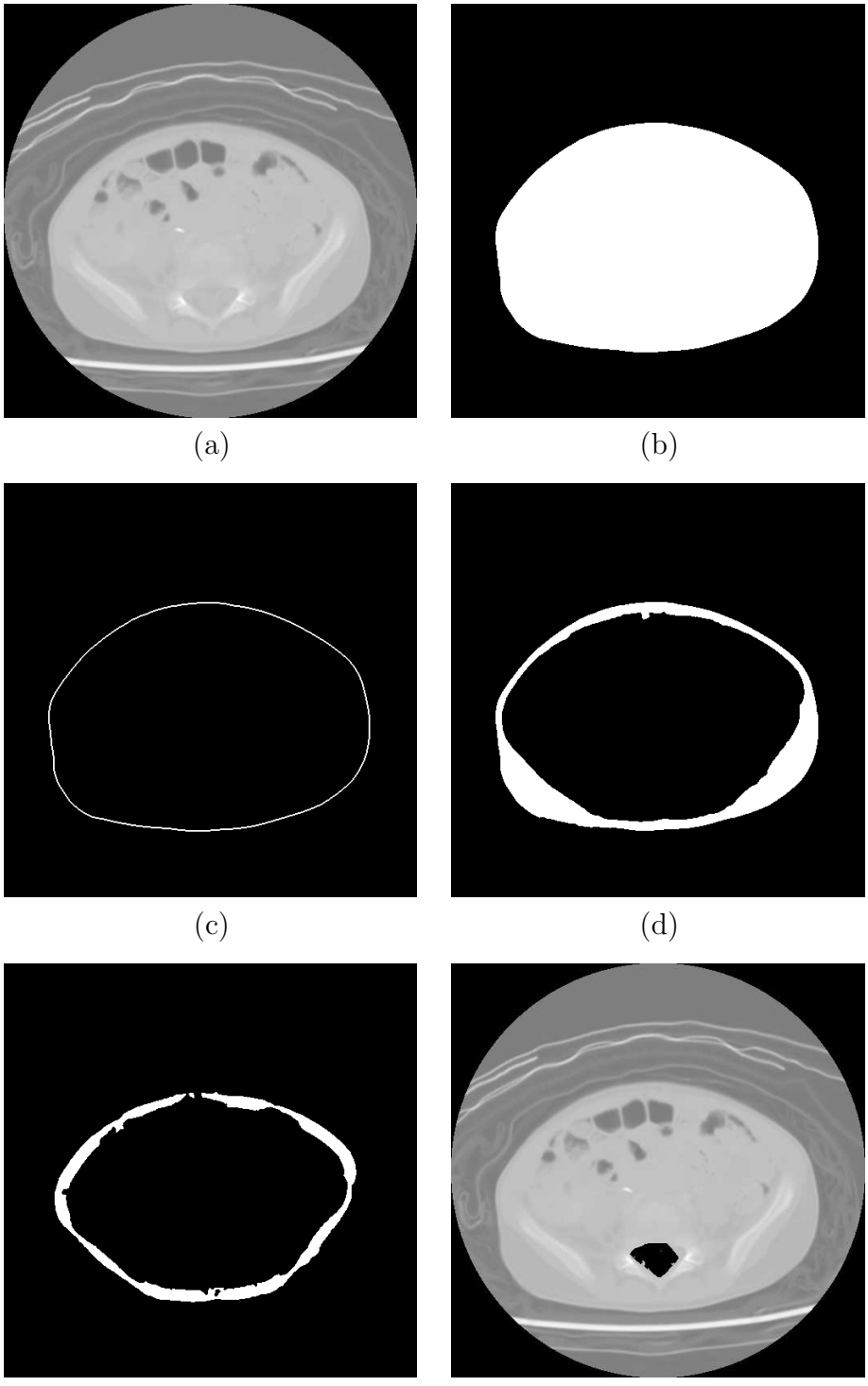

Figure 1: (a) A 512×512 CT slice of a patient. Only one cross section is shown from an exam with 75 slices. (b)External air and artifacts(shown in black). (c) The peripheral skin. (d) The peripheral fat region. (e) The pheripheral muscle region. (f) The spinal canal region detected and removed.

for the left part of pelvic girdle was defined within $100-200$ in X-axis direction and $250-350$ in Y-axis direction in the thresholded image. And for the right part of the pelvic girdle, it was

defined within $350 - 450$ in X-axis direction and the $250 - 350$ in the Y-axis direction. The pixel that corresponds to 1 in the thresholded image and also very close to approximate mean value of 350 in the original image was taken as seed pixel. Though, there are some "magic numbers" here but for all the CT images the parts of the pelvic girdle was found within that region and the algorithm successfully been able to determine the seed pixels as expected.

For the case of three seed pixels, where the third one lies on the lower spine in the CT slice, was determined using the detected spinal canal mask. The center point (or the mean pixel) of the spinal canal mask in the same CT slice was determined and from that point I searched 30 pixels back in the Y-axis direction to get a seed on spine. This method also was able to determine an appropriate seed for spine for all the cases.

6.2 Methods Studied

I have used two appoaches two get the pelvic girdle: one with automatically selected seeds, fuzzy mapping and applying reconstruction along with other morphological processing and the second one is taking the fuzzy mapped air region as mask and eroding that region with a disk type structuring of radius 10 pixels used as a marker for reconstruction.

I have tested 4 similar procedures for the first approach depending on the number of seeds and application of region growing. The methods are described below.For all the images the upper 55% slices were not considered.

6.2.1 Method I

I have used 2 seeds simultaneously to get the right and left parts of pelvic girdle. The pre-processed image was mapped using the Equation 3 with an average mean value of 400 and average standard deviation of 120. These values were determined using a roughly estimated pelvic mask including bones and bone-marrows and for all the CT exams these values were found to be very close to the estimated value. Then using these seeds as point markers the reconstruction was applied with 26-connected neighborhood. Then the image was morphologically closed using a 'disk' type structuring element of radius 10 pixels and thresholded within the range 100 to 1200 HU. Then the binary image was dilated to fill the 'holes' using the same type of structuring elemnet of radius 3 pixels.

6.2.2 Method II

This method differs from the previous one in a manner that the seeds were used separately to do the reconstruction and then the obtained result was added to get the mask for right and left portions of the pelvis. The image was morphologically closed and dilated. After thresholding the binarized image was searched for the largest portion (labeling) and the resulted volume was closed again and thinned to get the mask for Pelvis. The structuring elements used for different morphological opearion were of disk type with a radius varying from 1 to 5 pixels depending on necessity.

The reason for labelling and finding largest region here is, when two separate results of region growing are merged, both the parts get connected somehow and I was not able to separate them without making any loss to the image of actual pelvis. So, I needed to take the opposite approach which in turns proved to be very optimistic about the pelvis boundary.

6.2.3 Method III

This method was implemented using 3 seeds simultaneously. The fuzzy mapped region was reconstructed with 26-connedted neighborhood using those seed points as marker. The reconstructed image was closed, dilated and labelled to find the maximum connected volume. Then the resulted mask was morphologically closed, filled and thinned to get the refined Pelvis mask.

6.2.4 Method IV

This method is same as Method II except 3 seeds are used to do the reconstruction separately. Following the same procedure of closing, dilation, thresholding, labelling and thinning the pelvic girdle mask was obtained.

6.2.5 Method V

In this method I have taken different approach which is little bit similar to *"closing by reconstruction"*. The fuzzy mapped air region was taken as the mask and that image eroded with a disk of radius 10 pixels was used as marker to perform the reconstruction with 6-connected neighborhood. The resulted image was inverted and closed by a disk of radius of 3 pixels. Then the image was eroded with the same structuring element to get a finer result.

7 Results

Based on the previously described methods some representative results are presented in Figures 2,3 and 4. Method-I is the simplest of all methods described here and it takes the lowest time to produce the output. This method has less leakage probabilty to other lower abdominal organs and produces very good result as seen in part (b) of 2. Another positive feature for this method is that it is designed to segment the two sides of the pelvic girdle though sometimes it includes the spine also. The disadvantage of this method is that it sometimes fails to produce good output at the lower end of the pelvis which is evident in part (b) of 4.

Method-II is designed such a way that it produces highly optimistic result about the pelvis. The inclusion of dilation is needed to get the maximum connected regions which has the negative effect of producing greater area for pelvis and also it produces huge leakage in abdominal structures of similar CT value (see part (c) of Figure 3). This method takes almost double time than the first method though it produces better estimation about the lower parts of pelvis.

Method-III produces similar output as in method-I with increased computational complexity and it also sometimes misses some lower parts of pelvis(see part (d) of Figure 4). And it has little higher probability of leakage and less possibility of missing lower parts than Method-I. The computation time is less than method-II but higher than method-I.

Method-IV is another optimistic representation which takes the highest time to produce output. It produces better estimation of the lower part compared to the previous three procedures and less likely to miss any parts. But it has very high possibility of leakage as in method-II.

Method-V results in good representation of pelvis and it also does not miss lower disjoint parts very often. The inclusion of other structures is highly possible if those contiguous structures have the close CT value. As it performs global operation similar to closing by

reconstruction, the upper threshold for air regions need to be manually adjusted (in between 40 to 180) to get a good result. Otherwise, for low contrast and small pelvic girdle region, the algorithm produces no meaningful output. The computaion time is as less as method-I.

The two major problems I have encountered in the project are the disjoint characteristics of the pelvis parts and similar CT characteristics of the neighboring regions. The inclusion of spine in the segmentation procedure is essential in many cases to get the lower portion of the pelvic girdle and to include the disjoint bones that belong to the pelvic girdle. But, that spine get connected most of the times to other organs and is one of the major reasons for high leakage during segmentation. Due to inclusion of contrast material in the abdominal organs, some of the structures show higher HU value than the normal. Due to noise and poor image quality and also for wanting to include the bone-marrows in the result to obtain a complete model of the pelvic girdle, result in poor representation by introducing high leakage.

Though it shouldn't cause much problem in region growing of bones directly, but those high contrast areas get connected to the low contrast pelvis regions and increase errors. Those problematic structures could be eliminated from the result by disconnecting from the pelvis region using erosion operation but it will cause the loss of pelvis parts also in the output. So, I had to make a compromise between these two criteria to obtain a good result.

8 Conclusion

The basic need for pelvic girdle detection fare to get the lower boundary of abdomen and remove all data below that region so that we will have only the segmented abdominal cavity to consider for region growing in the case of neuroblastoma. It has been observed that the region growing using fuzzy connectivity or opening by reconstruction leaks into some lower abdominal region in several cases giving rise to high false positive rates.

So, for the purpose of futher work in that field, only the upper surface region of the pelvic girdle is necessary. In that case, either Method-I or Method-III will be the best choice for implementaion in terms of producing a reliable result along with reduced computational complexity and time. Method-V also has some promising features but need to be refined for more reliable output.

Another thing about this project worth mentioning here that all the analysis are done in a subjective way. If there had been the accurate boundary defined by an expert radilogist or "ground truth" to compare the result with, it could be possible to make the analysis quantitive or more objective.

The automatic seed selection is a positive side for this study though that procedure still need to be made more reliable and logical for more number of CT exams. The only user input of these described methods is to select the upper bound of CT slices to consider for pelvic girdle. Though in this work, the upper 55% slices were removed before consideration, methods other than method-I starts to leak in the upper abdomen. To eliminate this problem, a manual upper bound (slice number) was defined by examining the slices to restrict the region growing. For this, selection of the upper limit of the considerable slices is need to be refined before starting pelvis segmenatation. The slice where the upper pelvic girdle starts to appear can be used to constraint the consideration.

Though method-I was found to be adequate to serve the purpose, other methods are also studied to find a complete representation of the whole pelvic girdle. In this purpose, other methods are extensively explored and compared to the method-I. In addition, the project

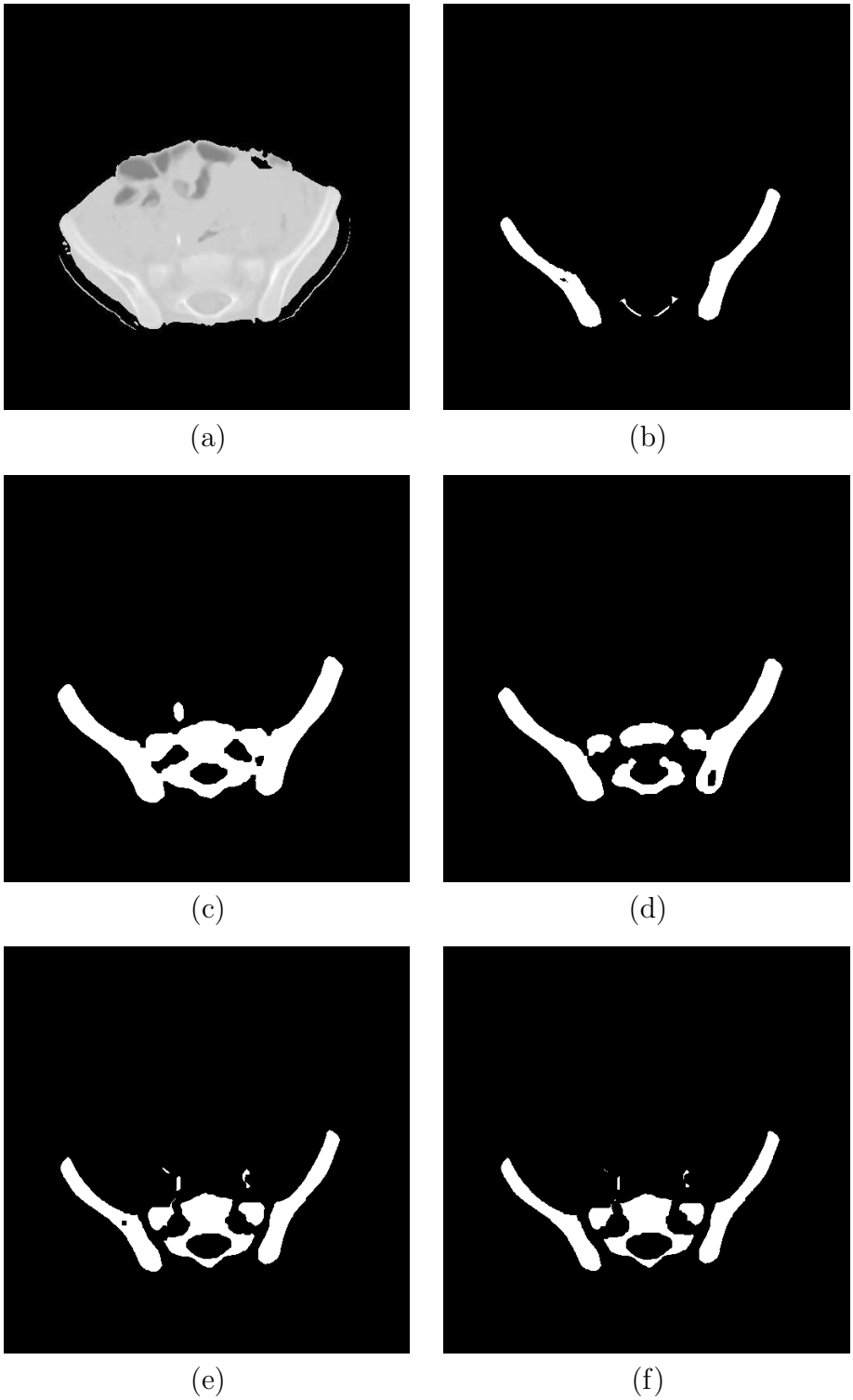

Figure 2: (a) A 512×512 CT slice after removal of air, skin, fat and muscle. Only one cross section is shown from an exam with 75 slices. (b) Mask obtained by Method-I; (c) Mask obtained by Method-II; (d) Mask obtained by Method-III; (e) Mask obtained by Method-IV; (f)Mask obtained by Method-V.

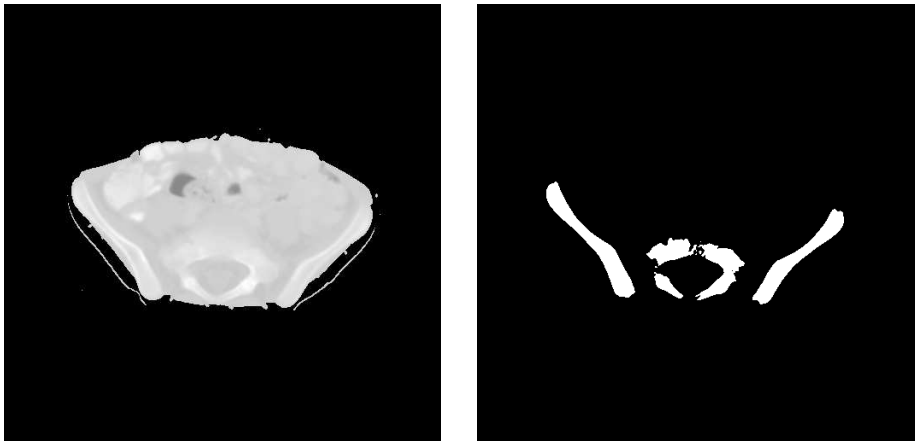

(a)

(b)

(c)

(d)

(e)

(f)

Figure 3: (a) A 512×512 CT slice after removal of air, skin, fat and muscle. Only one cross section is shown from an exam with 71 slices. (b) Mask obtained by Method-I; (c) Mask obtained by Method-II; (d) Mask obtained by Method-III; (e) Mask obtained by Method-IV; (f)Mask obtained by Method-V.

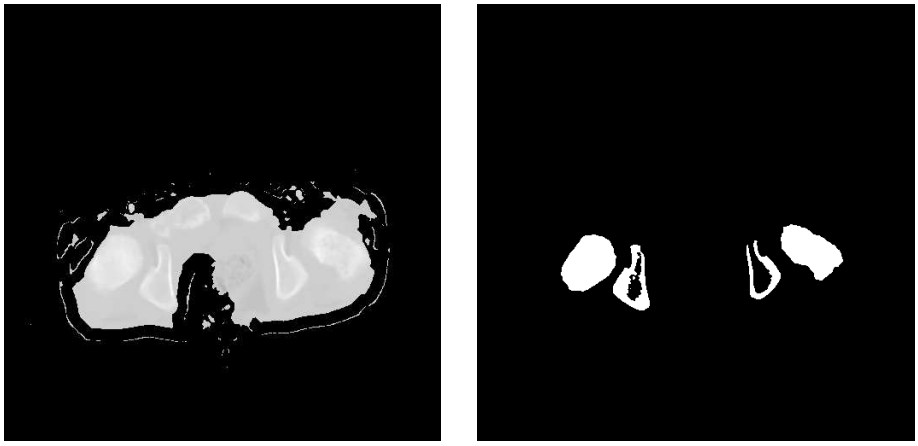

(a)

(b)

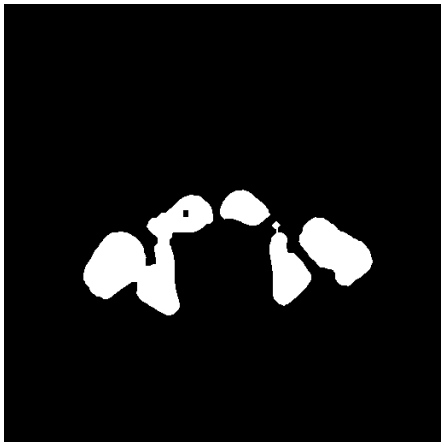

(c)

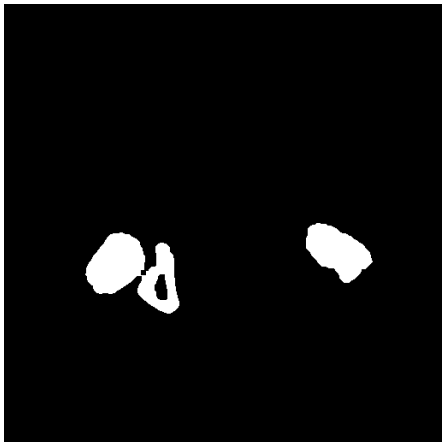

(d)

(e)

(f)

Figure 4: (a) A 512×512 CT slice after removal of air, skin, fat and muscle. Only one cross section is shown from an exam with 75 slices. (b) Mask obtained by Method-I; (c) Mask obtained by Method-II; (d) Mask obtained by Method-III; (e) Mask obtained by Method-IV; (f)Mask obtained by Method-V

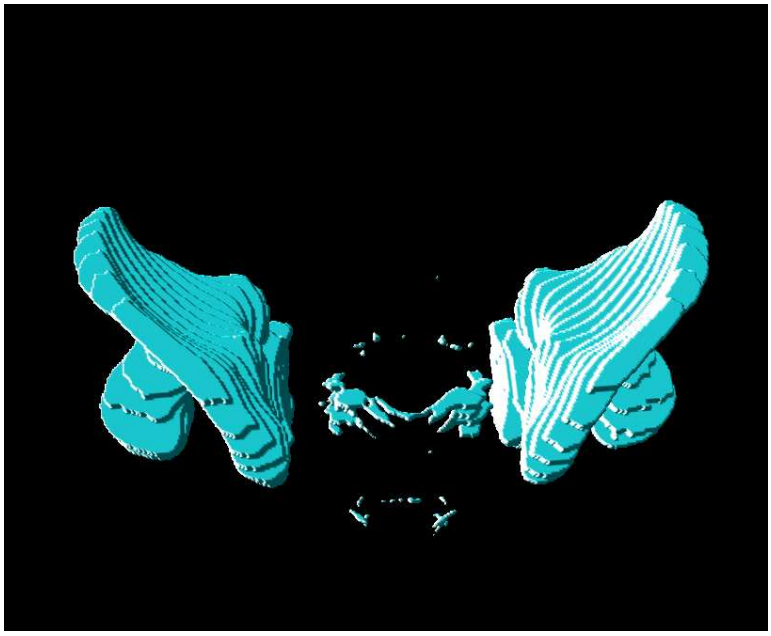

(a)

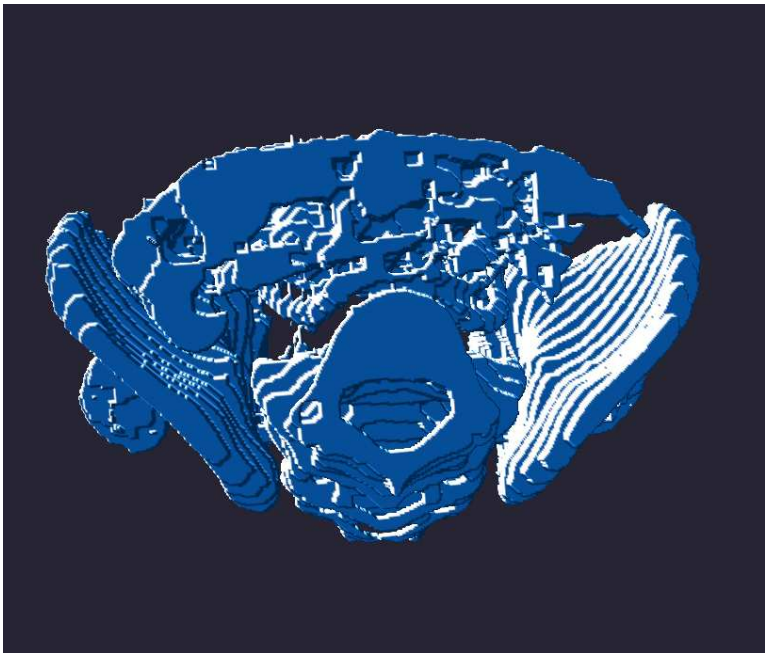

(b)

Figure 5: Two representative cases in 3D (top view)(a) Pelvis surface obtained by method-I; (b) Pelvis surface obtained with method-IV.

was formed in a manner with a view to set up an initial learning point of biomedical image processing for myself and building up a good background for future work in this field.

9 Future Work

My future aims related to this project are:

* To refine the method of pelvic girdle detection and segmentation.

* To implement simultaneous and competitive region growing method to segment the primary tumor mass in neuroblastoma.

* To determine the tissue composition in the tumor mass using Gaussian Mixture model

* To find a more reliable and successful algorithm for the segmentation of neuroblastoma using more imaging modalities including μmeter resolution CT images.

* To extend the study for other abdominal cancers like Wilm's tumor etc.

* To try to find a complete automated procedure of segmentation of abdominal tumors.

References

[1] F Alexander. Neuroblastoma. *Urologic Clinics of North America*, 27(3):383–392, August 2000.

[2] S J Abramson. Adrenal neoplasms in children. *Radiologic Clinics of North America*, 35(6):1415–1453, 1997.

[3] A Bousvaros, D R Kirks, and H Grossman. Imaging of neuroblastoma: an overview. *Pediatric Radiology*, 16:89–106, 1986.

[4] J L Grosfeld. Risk-based management of solid tumors in children. *The American Journal of Surgery*, 180:322–327, November 2000.

[5] G M Brodeur, R G Seeger, A Barrett, F Berthold, R P Castleberry, G D'Angio, B DeBernardi A E, Evans, M Favrot, A I Freeman, G Haase, O Hartmann, F A Hayes, L Helson, J Kemshead, F Lampert, J Ninane, H Ohkawa, T Philip, C R Pinkerton, J Pritchard, T Sawada, S Siegel, E I Smith, Y Tsuchida, and P A Voûte. International criteria for diagnosis, staging, and response to treatment in patients with neuroblastoma. *Journal of Clinical Oncology*, 6(12):1874–1881, December 1988.

[6] Canadian Cancer Society. Canadian cancer statistics 2004. Technical report, National Cancer Institute of Canada, Toronto, Canada, 2004.

[7] J R Sty, R G Wells, R J Starshak, and D C Gregg. *Diagnostic Imaging of Infants and Children*, volume I. Aspen Publishers, Inc., Gaithersburg, MD, 1992.

[8] R P Castleberry. Neuroblastoma. *European Journal of Cancer*, 33(9):1430–1438, 1997.

[9] J M Michalski. Neuroblastoma. In C A Perez, L W Brady, E C Halperin, and R K Schmidt-Ullrich, editors, *Principles and Practice of Radiation Oncology*, pages 2247–2260. Lippincott Williams and Wilkins, Philadelphia, PA, 4th edition, 2004.

[10] G M Brodeur, J Pritchard, F Berthold, N L T Carlsen, V Castel, R P Castleberry, B DeBernardi, A E Evans, M Favrot, F Hedborg, M Kaneko, J Kemshead, F Lampert, R E J Lee, A T Look, A D J Pearson, T Philip, B Roald, T Sawada, R C Seeger, Y Tsuchida, and P A Voûte. Revisions of the international criteria for neuroblastoma diagnosis, staging, and response to treatment. *Journal of Clinical Oncology*, 11(8):1466–1477, August 1993.

[11] B H Kushner. Neuroblastoma: A disease requiring a multidude of imaging studies. *Journal of Nuclear Medicine*, 45:101–105, July 2004.

[12] F J Ayres, M K Zuffo, R M Rangayyan, G S Boag, V Odone Filho, and M Valente. Estimation of the tissue composition of the tumor mass in neuroblastoma using segmented CT images. *Medical and Biological Engineering and Computing*, 42:366–377, 2004.

[13] Rangaraj M. Rangayyan H.J. Deglint and G.S. Boag. Three-dimensional segmentation of the tumor mass in computed tomographic images of neuroblastoma. *Proceedings of the SPIE Intenational Symposium on Medical Imaging: Image Processing*, 5370(3):475–483(2004), May 2004.

[14] H.J. Deglint. Image processing algorithm for three-dimensional segmentation of the tumor mass in computed tomographic images of neuroblastoma. Master's thesis, University of Calgary, August 2004.

[15] Randy Hoang Vu. Strategies for three-dimensional segmentation of the primary tumor mass in computed tomographic images of neuroblastoma. Master's thesis, University of Calgary, July 2006.

[16] P K Sahoo, S Soltani, A K C Wong, and Y C Chen. A survey of thresholding techniques. *Computer Vision, Graphics, and Image Processing*, 41:233–260, 1988.

[17] J K Udupa and S Samarasekera. Fuzzy connectedness and object definition: Theory, algorithms, and applications in image segmentation. *Graphical Models and Image Processing*, 58(3):246–261, 1996.

[18] I Bloch. Fuzzy connectivity and mathematical morphology. *Pattern Recognition Letters*, 14:483–488, 1993.

[19] C R Giardina. *Morphological Methods in Image and Signal Processing.* Prentice Hall, Englewood Cliffs, NJ, 1988.

[20] E R Dougherty. *An Introduction to Morphological Image Processing.* SPIE Press, Bellingham, WA, 1992.

[21] J Goutsias and S Batman. Morphological methods for biomedical image analysis. In M Sonka and J M Fitzpatrick, editors, *Handbook of Medical Imaging, Volume 2: Medical Image Processing and Analysis*, pages 175–272. SPIE Press, Bellingham, WA, 2000.

[22] L Vincent. Morphological grayscale reconstruction in image analysis: Applications and efficient algorithms. *IEEE Transactions on Image Processing*, 2(2):176–201, 1993.

[23] V C Mategrano, J Petasnick, J Clark, A C Bin, and R Weinstein. Attenuation values in computed tomography of the abdomen. *Radiology*, 125:135–140, October 1977.

[24] M E Phelps, E J Hoffman, and M M Ter-Pogossian. Attenuation coefficients of various body tissues, fluids and lesions at photon energies of 18 to 136 keV. *Radiology*, 117:573–583, December 1975.